Neutrino-nucleus reactions on ^{16}O based on new shell-model Hamiltonians

Toshio Suzuki,[1,2,*] Satoshi Chiba,[3] Takashi Yoshida,[4] Koh Takahashi,[5] and Hideyuki Umeda[4]

[1]*Department of Physics, College of Humanities and Sciences, Nihon University Sakurajosui 3-25-40, Setagaya-ku, Tokyo 156-8550, Japan*

[2]*National Astronomical Observatory of Japan, Mitaka, Tokyo 181-8588, Japan*

[3]*Research Laboratory for Nuclear Reactors, Tokyo Institute of Technology, Meguro, Tokyo 152-8550, Japan*

[4]*Department of Astronomy, Graduate School of Science, The University of Tokyo, Hongo, Bunkyo-ku, Tokyo 113-0033, Japan*

[5]*Argelander-Institute für Astronomie, Universität Bonn, D-53121 Bonn, Germany*

(Received 5 July 2018; revised manuscript received 4 September 2018; published 28 September 2018)

Neutrino-induced reactions on ^{16}O are investigated by shell-model calculations with new shell-model Hamiltonians, which can describe well the structure of p-shell and p-sd-shell nuclei. The distribution of the spin-dipole strengths in ^{16}O, which give major contributions to the ν-^{16}O reaction cross sections, is studied with the new Hamiltonians. Muon-capture reaction rates on ^{16}O are also studied to discuss the quenching of the axial-vector coupling in the nuclear medium. Charged-current and neutral-current reaction cross sections are evaluated in various particle and γ emission channels as well as the total ones at neutrino energies up to $E_\nu \approx 100$ MeV. Branching ratios for the various channels are obtained by the Hauser-Feshbach statistical model calculations, and partial cross sections for single- and multiparticle emission channels are evaluated. The cross sections updated are compared with previous continuum random phase approximation calculations. Effects of multiparticle emission channels on nucleosynthesis in core-collapse supernova explosions are investigated. Inclusion of αp emission channels is found to lead to an enhancement of production yields of ^{11}B and ^{11}C through ^{16}O$(\nu, \nu'\alpha p)^{11}$B and ^{16}O$(\nu_e, e^-\alpha p)^{11}$C reactions, respectively.

DOI: 10.1103/PhysRevC.98.034613

I. INTRODUCTION

The study of neutrino-nucleus reactions at neutrino energies up to $E_\nu = 100$ MeV is an important subject for the detection of supernova (SN) neutrinos. Several nuclear targets such as ^{12}C, ^{16}O, and ^{40}Ar are especially of interest from the point of view of their availability. Accurate evaluation of the ν-induced cross sections is crucial for the study of neutrino production and nucleosynthesis in SN explosions as well as neutrino oscillation properties.

Recently, new shell-model Hamiltonians became available due to the development of the study of exotic nuclei. Important roles of the tensor interaction are taken into account in the new Hamiltonians, so that they can explain shell evolutions and the change of magic numbers toward driplines [1,2]. Spin modes of nuclei such as Gamow-Teller (GT) transitions and magnetic dipole transitions and moments are found to be well described by these Hamiltonians.

Neutrino-induced reaction cross sections on ^{12}C have been evaluated with a new p-shell Hamiltonian, SFO (named for Suzuki, Fujimoto, and Otsuka) [3], which can reproduce the GT transition strength in ^{12}C. The SFO is constructed to be used in p-sd shell with the inclusion of excitations of p-shell nucleons to the sd shell up to $2\hbar\omega$–$3\hbar\omega$ configurations. Exclusive and inclusive charged- and neutral-current reaction cross sections for decay-at-rest (DAR) ν's are found to be well reproduced by the SFO within experimental error bars [4,5]. Cross sections for particle emission channels obtained by the Hauser-Feshbach method are used to study nucleosynthesis of light elements in SN explosions [4,6]. Production yields of ^{7}Li and ^{11}B are found to be enhanced compared with previous calculations [7]. In the case of Mikheyev-Smirnov-Wolfenstein (MSW) resonance ν oscillations, the yield ratio of ^{7}Li/^{11}B is pointed out to be a good measure of neutrino mass hierarchy [5,6,8].

The same Hamiltonian, SFO, is applied to ν-induced reactions on ^{13}C. The ^{13}C isotope, whose abundance in carbon isotopes is 1.1%, is a favorable target for detection of low energy ν below $E_\nu \sim 10$ MeV, as reaction cross sections on ^{12}C vanish below $E_\nu = 15$ MeV. The updated cross sections for ^{13}C are found to be enhanced compared with those of Cohen-Kurath interactions [9,10].

Since liquid argon is an important target for the ν detection, accurate evaluation of ν-induced cross sections on ^{40}Ar is crucial for the study of SN neutrinos. Charged-current cross sections on ^{40}Ar have been evaluated with the use of recent new shell-model Hamiltonians. Phenomenological Hamiltonians, SDPF-M [11] and GXPF1J [12], are adopted for sd and pf shells, respectively, while the monopole-based universal interaction [2] is used to obtain the sd-pf cross shell matrix elements. The GT strength in ^{40}Ar obtained in (p, n) reactions [13] is reproduced rather well by the shell-model calculations [14]. The GT strength is found to be large compared with a previous shell-model estimation [15]. The cross section for ^{40}Ar is enhanced at $E_\nu < 50$ MeV, where the GT transitions

*suzuki@chs.nihon-u.ac.jp

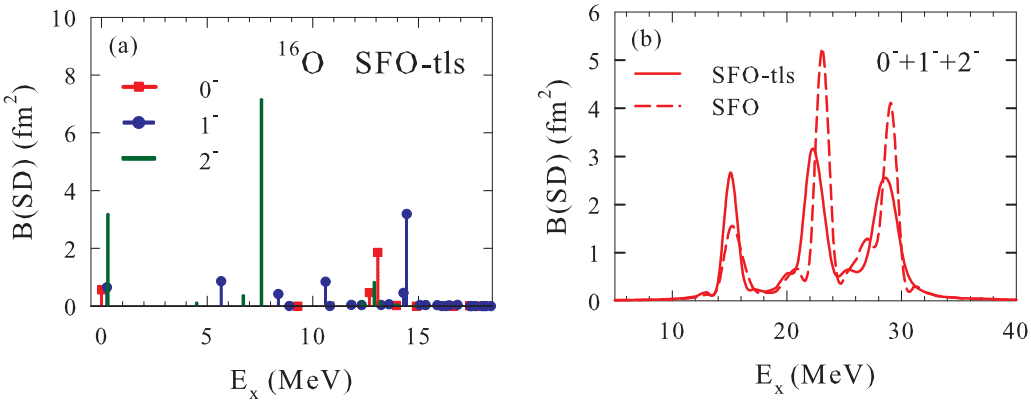

FIG. 1. (a) Spin-dipole strengths for ^{16}O → ^{16}F obtained by shell-model calculations with SFO-tls. E_x denotes the excitation energy of ^{16}F. (b) Comparison of the spin-dipole strengths for ^{16}O → ^{16}F obtained with SFO-tls and those with SFO. The strengths are folded over a Lorentzian with a width of 1 MeV. E_x denotes the excitation energy of ^{16}O.

are dominant. In addition to 1^+ and 0^+ transitions, cross sections are evaluated with the random-phase approximation (RPA). The contributions from multipoles with 0^-, 1^-, and 2^- become important at $E_\nu > 50$ MeV. The cross section by the hybrid model is enhanced by about 20–40% compared to that obtained by RPA [16] at lower energies, $E_\nu < 40$ MeV.

Here, we study ν-induced reactions on ^{16}O, which is the content of the water target and is expected to be promising for SN neutrino detection [17]. In Sec. II, we investigate spin-dipole transition strengths in ^{16}O based on new shell-model Hamiltonians, and discuss quenching of the axial-vector coupling of weak hadronic interaction in the nuclear medium by studying the muon-capture reaction on ^{16}O. In Sec. III, charged- and neutral-current reaction cross sections are evaluated by shell-model calculations. Total and partial cross sections for various particle and γ emission channels are obtained and compared with previous calculations [17]. In Sec. IV, we discuss nucleosynthesis of ^{11}B and ^{11}C produced by emissions of α and protons from ^{16}O in SN explosions. The summary is given in Sec. V.

II. SPIN-DIPOLE STRENGTHS IN ^{16}O

The shell-model Hamiltonian for the p shell, SFO, has been successfully applied to the GT transitions in ^{12}C. The tensor components are properly improved in the p-shell part of SFO by enhancing the monopole terms in the spin-isospin flip channel. In the case of ^{16}O, the GT transition gives only a minor contribution as ^{16}O is an LS-closed shell nucleus, that is, the spin-orbit partner orbits of the core are completely occupied. Dominant contributions come from spin-dipole (SD) transitions, where p-shell nucleons are excited into the sd shell. Thus, the p-sd cross-shell interaction plays an important role. The p-sd shell cross-shell part of SFO is a phenomenological Millener-Kurath interaction [18]. It is important to update the p-sd cross-shell part of the Hamiltonian with proper inclusion of the tensor interaction. Here, we use a modified version of SFO, in which the tensor and two-body spin-orbit components of the p-sd cross-shell matrix elements are replaced by those of $\pi + \rho$ meson exchanges and $\sigma + \omega + \rho$ meson exchanges [19], respectively. The modified Hamiltonian, referred as SFO-tls [20], has been found to describe well the structure of neutron-rich carbon isotopes [20,21].

Spin-dipole strengths with λ^π are defined as

$$B(\mathrm{SD}\lambda)_\mp = \frac{1}{2J_i+1}\sum_f |\langle f\|S^\lambda_\mp\|i\rangle|^2,$$
$$S^\lambda_{\mp,\mu} = r[Y^1\times\vec{\sigma}]^\lambda_\mu t_\mp, \qquad (1)$$

where J_i is the spin of the initial state and $t_-|n\rangle = |p\rangle$ and $t_+|p\rangle = |n\rangle$. Calculated spin-dipole strengths for ^{16}O($0^+_{g.s.}$) → ^{16}F($\lambda^\pi = 0^-, 1^-, 2^-$) obtained with SFO-tls as well as SFO are shown in Fig. 1. Configurations up to $3\hbar\omega$ ($2\hbar\omega$) excitations from p shell to sd shell are included for the spin-dipole (ground) states. Experimental energies of the lowest 0^-, 1^-, f and 2^- states, $E_x = 0.0$, 0.194, and 0.425 MeV, respectively [22], are rather well reproduced by shell-model calculations with SFO-tls. Calculated energies are $E_x = 0.0$, 0.251, and 0.299 MeV for 0^-, 1^-, and 2^- states, respectively, which agree with the experimental values within 0.13 MeV. The 2^- state at $E_x = 7.50$ MeV, which has the largest strength among the spin-dipole states, is located at the right position with $E_x = 7.57$ MeV for the SFO-tls. In the case of the SFO, the calculated energy of the corresponding 2^- state is $E_x = 8.27$ MeV, higher than the observed energy by 0.7 MeV. The energy of the lowest 2^- state for the SFO is $E_x = 0.705$ MeV, which is also higher than the experimental value by 0.28 MeV. The spin-dipole strengths for the SFO are shifted toward the higher energy region by 0.3–1 MeV compared with those for the SFO-tls as shown in Fig. 1(b).

Sum rule values of the SD strength in ^{16}O are given by using the harmonic oscillator wave functions as [23]

$$S_\lambda(\mathrm{SD}) = \sum_\mu |\langle\lambda,\mu|S^\lambda_{-,\mu}|0\rangle|^2$$
$$= \begin{cases} \frac{3}{4\pi}4b^2 = 2.99\ \mathrm{fm}^2, & \lambda^\pi = 0^-, \\ \frac{3}{4\pi}12b^2 = 8.98\ \mathrm{fm}^2, & \lambda^\pi = 1^-, \\ \frac{3}{4\pi}20b^2 = 14.96\ \mathrm{fm}^2, & \lambda^\pi = 2^-, \end{cases} \qquad (2)$$

where the excitations from p to sd shells are considered and the oscillator parameter is taken to be $b = 1.77$ fm^2. The SD strength for SFO-tls below $E_x = 40$ MeV exhausts 99%, 77%, and 82% of the sum rule values for 0^-, 1^-, and 2^-, respectively. As the tensor interaction shifts the 1^- (0^- and 2^-) strength to the higher (lower) energy region, the summed fraction up to $E_x = 40$ MeV for 1^- is smaller than those for 0^- and 2^-.

The energy-weighted sum (EWS) of the spin-dipole operator in Eq. (1), defined by

$$\mathrm{EWS}^{\lambda}_{\pm} = \sum_{\mu} |\langle \lambda, \mu | S^{\lambda}_{\pm,\mu} | 0 \rangle|^2 (E_\lambda - E_0), \tag{3}$$

is used to obtain

$$\begin{aligned} \mathrm{EWS}^{\lambda} &= \mathrm{EWS}^{\lambda}_{-} + \mathrm{EWS}^{\lambda}_{+} \\ &= \tfrac{1}{2} \langle 0 | [S^{\lambda\dagger}_{-}, [H, S^{\lambda}_{-}]] + [[S^{\lambda\dagger}_{+}, H], S^{\lambda}_{+}] | 0 \rangle. \end{aligned} \tag{4}$$

The EWS rule value for the kinetic energy term (K) for $H = \frac{p^2}{2m}$ with m the nucleon mass is given as [24]

$$\mathrm{EWS}^{\lambda}_{K} = \frac{3}{4\pi}(2\lambda+1)\frac{\hbar^2}{2m} A \left[1 + \frac{f_\lambda}{3A} \langle 0 | \sum_i \vec{\sigma}_i \cdot \vec{\ell}_i | 0 \rangle \right], \tag{5}$$

where $f_\lambda = 2$, 1, and -1 for $\lambda^\pi = 0^-$, 1^-, and 2^-, respectively. For LS-closed nuclei, the last term in Eq. (5) vanishes. The EWS rule value for the one-body spin-orbit potential (LS), $V_{\mathrm{LS}} = -\xi \sum_i \vec{\ell}_i \cdot \vec{\sigma}_i$, is given as [24]

$$\mathrm{EWS}^{\lambda}_{\mathrm{LS}} = \frac{3}{4\pi}(2\lambda+1)\frac{f_\lambda}{3}\xi \langle 0 | \sum_i \left(r_i^2 + g_\lambda r_i^2 \vec{\ell}_i \cdot \vec{\sigma}_i \right) | 0 \rangle, \tag{6}$$

where $g_\lambda = 1$ for $\lambda^\pi = 0^-$, 1^- and $g_\lambda = -7/5$ for $\lambda^\pi = 2^-$. Note that $\mathrm{EWS}^{\lambda=2}_{\mathrm{LS}}$ is reduced by the spin-orbit potential. For an LS-closed ^{16}O, $\langle 0 | \sum_i \vec{\ell}_i \cdot \vec{\sigma}_i | 0 \rangle = 0$, $\langle 0 | \sum_i r_i^2 \vec{\ell}_i \cdot \vec{\sigma}_i | 0 \rangle = 0$, and $\mathrm{EWS}^{\lambda}_{-} = \mathrm{EWS}^{\lambda}_{+}$. Then, with $\xi = 1.87$ MeV [25], $\mathrm{EWS}^{\lambda}_{-}$ for $K + \mathrm{LS}$ terms are obtained to be 56.4, 144.1, and 155.9 MeV fm^2 for 0^-, 1^-, and 2^-, respectively.

Values of $\mathrm{EWS}^{\lambda}_{-}$ obtained by the shell-model calculations including up to $3\hbar\omega$ excitations are 73.0 (76.1), 173.2 (175.0), and 246.5 (258.2) MeV fm^2 for the SFO-tls (SFO) for $\lambda^\pi = 0^-$, 1^-, and 2^-, respectively. The contributions up to $E_x \approx 50$ MeV are included. The shell-model values of $\mathrm{EWS}^{\lambda}_{-}$ are enhanced compared with those of the $K + \mathrm{LS}$ terms by 1.29 (1.35) for 0^-, by 1.20 (1.21) for 1^-, and by 1.58 (1.66) for 2^- in case of the SFO-tls (SFO). These enhancements are caused by the contributions from two-body spin-dependent interactions, especially the tensor interaction in the shell-model Hamiltonians. The enhancement factor is noticed to be large for 2^-, where the tensor interaction works attractively to shift the spin-dipole strength to lower energy region. This can be shown also from the centroid energy of the strength defined by $\bar{E}_\lambda = \mathrm{EWS}^{\lambda}_{-}/\mathrm{NEWS}^{\lambda}_{-}$, where $\mathrm{NEWS}^{\lambda}_{-}$ is the calculated value of S_λ(SD). Values obtained for the SFO-tls (SFO) are $\bar{E}_0 = 24.5$ (25.8), $\bar{E}_1 = 25.1$ (25.2), and $\bar{E}_2 = 20.1$ (21.0) MeV. Splitting of the centroid energies reflects attractive (repulsive) effects of the spin-dependent interaction in $\lambda^\pi = 0^-$ and 2^- ($\lambda^\pi = 1^-$). The shift of $\bar{E}_0$ and $\bar{E}_2$ to lower energies by 0.7–0.9 MeV from SFO to SFO-tls comes from the effects of the tensor interaction properly taken into account in the p-sd cross-shell part in the SFO-tls.

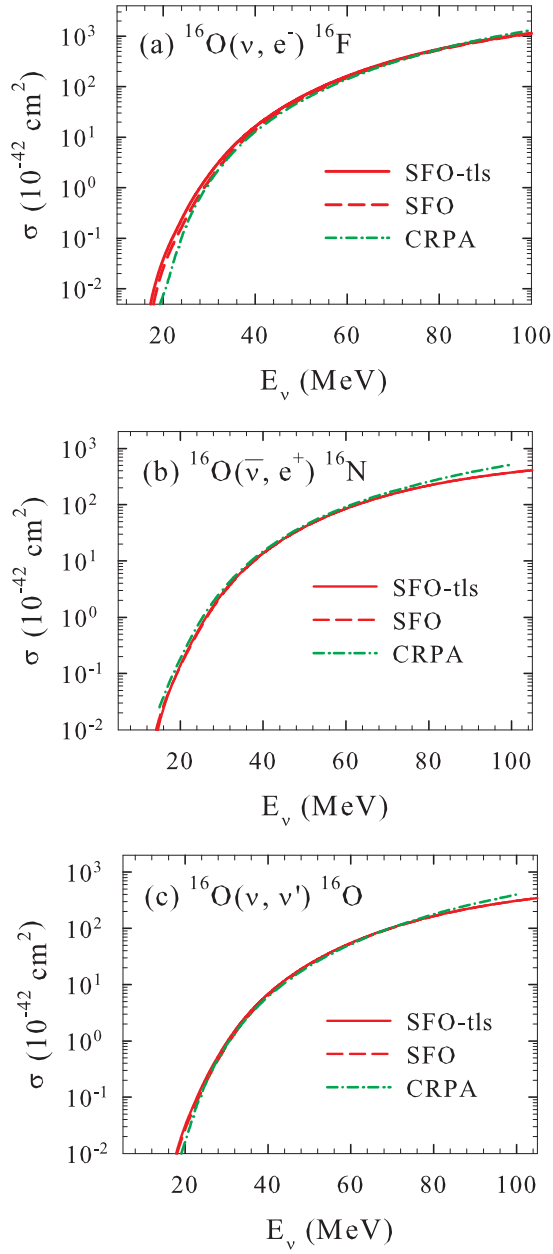

FIG. 2. Total reaction cross sections for (a) ^{16}O(ν_e, e^-)^{16}F, (b) ^{16}O ($\bar{\nu}_e, e^+$)^{16}N, and (c) ^{16}O(ν, ν')^{16}O obtained by shell-model calculations with the SFO-tls and SFO as well as those of the CRPA calculation [17].

Next, we discuss quenching of the axial-vector coupling constant g_A in the nuclear medium in order to get a reliable evaluation of ν-induced reaction cross sections on ^{16}O. A quenching factor of $f = g_A^{\mathrm{eff}}/g_A = 0.95$ close to 1.0 is obtained for the SFO from the study of the GT transition in ^{12}C [3]. Magnetic moments of p-shell nuclei are found to be systematically well reproduced with the use of this quenching factor for the isovector spin g-factor [3]. In the case

TABLE I. Total ν-induced cross sections on ^{16}O obtained with the SFO-tls, SFO, and CRPA. The cross sections are given in units of 10^{-42} cm^2 as a function of the incoming neutrino energy E_ν. Exponents are given in parentheses.

E_ν (MeV)	^{16}O(ν_e, e^-)^{16}F			^{16}O($\bar{\nu}_e$, e^+)^{16}N			^{16}O(ν, ν')^{16}O		
	SFO-tls	SFO	CRPA	SFO-tls	SFO	CRPA	SFO-tls	SFO	CRPA
15.0	0.0	0.0	1.56(−6)	1.33(−2)	1.65(−2)	2.53(−2)	6.05(−4)	6.06(−4)	5.10(−4)
20.0	3.76(−2)	2.51(−2)	7.26(−3)	1.38(−1)	1.32(−1)	1.81(−1)	3.10(−2)	2.61(−2)	1.60(−2)
25.0	3.50(−1)	2.48(−1)	1.77(−1)	7.09(−1)	6.57(−1)	8.90(−1)	2.15(−1)	1.79(−1)	1.75(−1)
30.0	1.82(+0)	1.38(+0)	1.25(+0)	2.56(+0)	2.43(+0)	2.94(+0)	9.34(−1)	8.05(−1)	8.43(−1)
35.0	6.30(+0)	5.16(+0)	4.76(+0)	6.61(+0)	6.41(+0)	7.26(+0)	2.89(+0)	2.61(+0)	2.59(+0)
40.0	1.62(+1)	1.40(+1)	1.28(+1)	1.38(+1)	1.35(+1)	1.48(+1)	6.80(+0)	6.34(+0)	6.09(+0)
45.0	3.40(+1)	3.05(+1)	2.76(+1)	2.48(+1)	2.45(+1)	2.64(+1)	1.34(+1)	1.27(+1)	1.21(+1)
50.0	6.26(+1)	5.74(+1)	5.21(+1)	4.02(+1)	4.00(+1)	4.29(+1)	2.33(+1)	2.24(+1)	2.14(+1)
55.0	1.04(+2)	9.72(+1)	8.89(+1)	6.03(+1)	6.01(+1)	6.46(+1)	3.71(+1)	3.60(+1)	3.46(+1)
60.0	1.61(+2)	1.52(+2)	1.41(+2)	8.51(+1)	8.50(+1)	9.17(+1)	5.51(+1)	5.37(+1)	5.24(+1)
65.0	2.35(+2)	2.24(+2)	2.12(+2)	1.14(+2)	1.14(+2)	1.25(+2)	7.72(+1)	7.57(+1)	7.53(+1)
70.0	3.26(+2)	2.93(+2)	3.02(+2)	1.47(+2)	1.47(+2)	1.63(+2)	1.03(+2)	1.02(+2)	1.04(+2)
80.0	5.54(+2)	5.37(+2)	5.52(+2)	2.20(+2)	2.20(+2)	2.57(+2)	1.65(+2)	1.64(+2)	1.78(+2)
90.0	8.34(+2)	8.15(+2)	8.92(+2)	2.97(+2)	2.98(+2)	3.77(+2)	2.36(+2)	2.35(+2)	2.76(+2)
100.0	1.14(+3)	1.13(+3)	1.32(+3)	3.74(+2)	3.75(+2)	5.18(+2)	3.10(+2)	3.09(+2)	3.99(+2)

of the SFO-tls, almost the same quenching factor, $f = 0.96$, is obtained to reproduce the GT strength in ^{12}C. Here, we study muon capture on ^{16}O to obtain information on the quenching factor in the spin-dipole transitions.

The muon-capture rate for ^{16}O(μ, ν_μ)^{16}N from the $1s$ Bohr atomic orbit is given as [26]

$$\omega_\mu = \frac{2G^2}{1+\nu/M_T}|\phi_{1s}|^2 \frac{1}{2J_i+1}\left(\sum_{J=0}^{\infty}|\langle J_f\|M_J - L_J\|J_i\rangle|^2 + \left|\langle J_f\|T_J^{\rm el} - T_J^{\rm mag}\|J_i\rangle\right|^2\right), \quad (7)$$

where $G = G_F \cos\theta_C$ is the weak-coupling constant with G_F the Fermi constant, θ_C the Cabibbo angle, ν the neutrino energy, M_T the target mass, and

$$|\phi_{1s}|^2 = \frac{R}{\pi}\left(\frac{m_\mu M_T}{m_\mu + M_T} Z\alpha\right)^3, \quad (8)$$

where m_μ is the muon mass, α is the fine-structure constant, $Z = 8$, and R is a reduction factor to take into account the finite nuclear size effect. A value of $R = 0.79$ is adopted for ^{16}O [26]. The transition matrix elements for the Coulomb (M_J), longitudinal (L_J), electric ($T_J^{\rm el}$), and magnetic ($T_J^{\rm mag}$) multipole operators with the multipolarities J are evaluated at the neutrino energy ν for the weak hadronic currents. In case of muon-capture reactions, there are sizable contributions from the pseudoscalar coupling term in the axial-vector current. The pseudoscalar form factor obtained from pion-pole dominance of the induced pseudoscalar coupling and the Goldberger-Treiman relation is used:

$$F_P(q_\mu^2) = \frac{2M_N}{q_\mu^2 + m_\pi^2} F_A(q_\mu^2), \quad (9)$$

where M_N is the nucleon mass, m_π is the pion mass, q_μ^2 is the four-momentum transfer, and F_A is the axial-vector form factor of the nucleon with $F_A(0) = -1.26$. Dominant

TABLE II. Averaged total ν-induced cross sections on ^{16}O over Fermi distributions of neutrino spectra with temperatures T. The cross sections are given in units of 10^{-42} cm^2 as a function of the temperature. Exponents are given in parentheses.

T (MeV)	^{16}O(ν_e, e^-)^{16}F			^{16}O($\bar{\nu}_e$, e^+)^{16}N			^{16}O(ν, ν')^{16}O		
	SFO-tls	SFO	CRPA	SFO-tls	SFO	CRPA	SFO-tls	SFO	CRPA
2	7.83(−3)	5.60(−4)		2.32(−3)	2.38(−3)		5.30(−4)	4.52(−4)	
3	2.97(−2)	2.35(−2)		4.42(−2)	4.27(−2)		1.52(−2)	1.42(−2)	
4	2.59(−1)	2.19(−1)	1.91(−1)	2.70(−1)	2.62(−1)		1.15(−1)	1.11(−1)	
5	1.13(+0)	9.96(−1)		9.44(−1)	9.22(−1)	1.05(+0)	4.61(−1)	4.53(−1)	
6	3.36(+0)	3.03(+0)		2.38(+0)	2.34(+0)	1.28(+0)	1.28(+0)		
7	7.79(+0)	7.17(+0)		4.88(+0)	4.82(+0)	2.81(+0)	2.84(+0)		
8	1.53(+1)	1.43(+1)	1.37(+1)	8.66(+0)	8.59(+0)	9.63(+0)	5.29(+0)	5.38(+0)	5.19(+0)
9	2.66(+1)	2.51(+1)		1.39(+1)	1.38(+1)		8.86(+0)	9.08(+0)	
10	4.23(+1)	4.02(+1)		2.06(+1)	2.05(+1)		1.37(+1)	1.41(+1)	

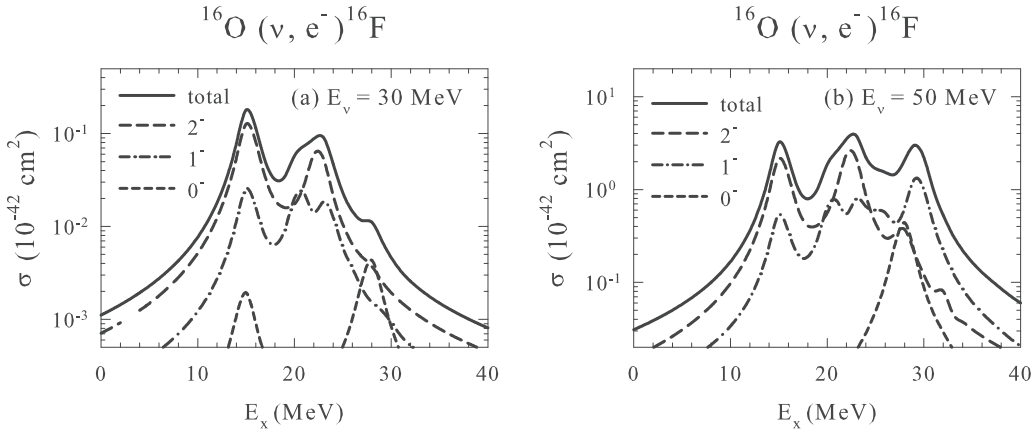

FIG. 3. Contributions from each 0^-, 1^-, and 2^- multipoles as well as the total cross sections for ^{16}O$(\nu_e, e^-)^{16}$F as a function of excitation energy E_x at (a) $E_\nu = 30$ MeV and (b) $E_\nu = 50$ MeV. The cross sections are folded over a Lorentzian with a width of 1 MeV.

contributions come from a region at $q_\mu^2 = m_\mu(2v\text{-}m_\mu) \approx (0.42\,\mathrm{fm}^{-1})^2$, for which $g_p = m_\mu F_P \approx 7.5$.

Total muon capture rates for ^{16}O obtained with $f = g_A^{\mathrm{eff}}/g_A = 0.95$ are 10.21×10^4 and 11.20×10^4 s^{-1} for the SFO and SFO-tls, respectively. They agree with the experimental value, 10.26×10^4 s^{-1} [27], within 10%. We thus find that nearly the same quenching factor $f \approx 0.95$ as in the GT transitions can be used also for the spin-dipole transitions within 10% accuracy for the strength. A quenching factor close to 1 has been also reported to be favorable for the continuum random phase approximation (CRPA) in Ref. [28].

III. NEUTRINO-INDUCED REACTION CROSS SECTIONS ON ^{16}O

A. Total cross sections

Neutrino-induced reaction cross sections are evaluated by using the multipole expansion of the weak hadronic currents,

$$J_\mu^{C_\mp} = J_\mu^{V_\mp} + J_\mu^{A_\mp}, \tag{10}$$

for charged-current reactions (ν, e^-) and $(\bar{\nu}, e^+)$, and

$$J_\mu^N = J_\mu^{A_3} + J_\mu^{V_3} - 2\sin^2\theta_W J_\mu^\gamma, \tag{11}$$

for neutral-current reactions, (ν, ν') and $(\bar{\nu}, \bar{\nu}')$, where J_μ^V and J_μ^A are vector and axial-vector currents, respectively, and J_μ^γ is the electromagnetic vector current with θ_W being the Weinberg angle. The reaction cross sections are given as the sum of the matrix elements of the Coulomb, longitudinal, and transverse electric and magnetic multipole operators for the vector and axial-vector currents [4,26]. Here, all the transition matrix elements with the multipolarities up to $\lambda = 4$ are taken into account with the use of harmonic oscillator wave functions. Initial and final states are obtained by the shell-model calculations in the p-sd shell configurations including up to 2 (3) $\hbar\omega$ excitations for the positive-parity (negative-parity) transitions. Excited states up to $E_x \approx 50$ MeV are taken into account.

First, we show results of total cross sections for charged- and neutral-current reactions: ^{16}O$(\nu_e, e^-)^{16}$F, ^{16}O$(\bar{\nu}_e, e^+)^{16}$N, and ^{16}O$(\nu, \nu')^{16}$O. Calculated cross sections for ^{16}O$(\nu_e, e^-)^{16}$F obtained with SFO-tls, SFO, and CRPA

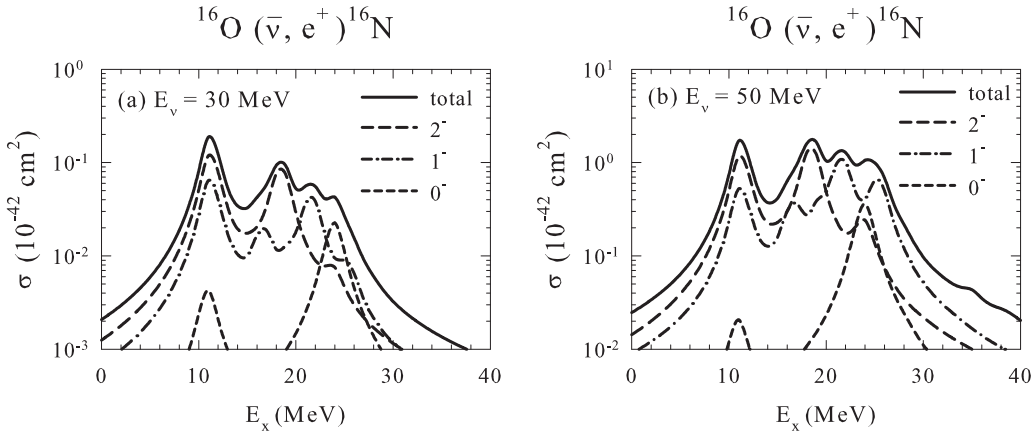

FIG. 4. The same as Fig. 3 for ^{16}O$(\bar{\nu}_e, e^+)^{16}$N.

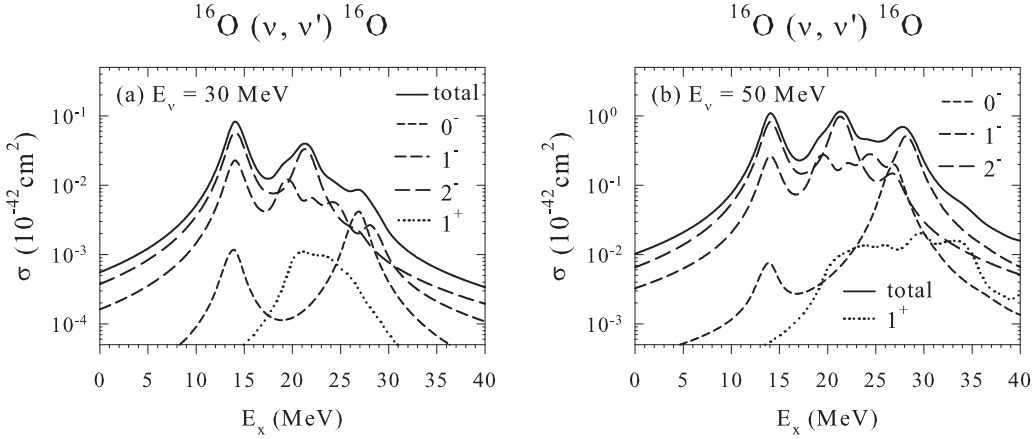

FIG. 5. The same as Fig. 3 for ^{16}O(ν, ν')^{16}O. Contributions from the 1^+ multipole are also shown.

[17] are shown in Fig. 2(a) as function of neutrino energy E_ν. The quenching factor for the axial-vector coupling constant is taken to be $g_A^{\rm eff}/g_A = 0.95$ for SFO-tls and SFO [3]. Calculated cross sections are summarized in Table I. The cross section for the SFO-tls is found to be enhanced compared with the CRPA at $E_\nu < 80$ MeV, and more than 50% at $E_\nu \leqslant 30$ MeV, while it becomes smaller than the CRPA at $E_\nu > 90$ MeV. The cross section for the SFO is close to the CRPA at $E_\nu = 30$–80 MeV. The enhancement of the cross section for the SFO-tls can be attributed to the shift of the SD strength to the lower excitation energy region compared to the SFO and CRPA. The cross sections for the SFO-tls and SFO are reduced compared to the CRPA at high E_ν as the CRPA calculations can take into account excited states with higher excitation energies than the shell-model calculations of the present *p-sd* shell configurations. The cross sections averaged over neutrino spectra of Fermi distributions with temperature T with zero chemical potential are given in Table II. The ratio of the cross sections, σ(SFO-tls)/σ(CRPA), is 1.36 (1.12) for $T = 4$ (8) MeV for ^{16}O(ν_e, e^-)^{16}F.

Total cross sections for ^{16}O($\bar\nu_e$, e^+)^{16}N and ^{16}O(ν, ν')^{16}O obtained with the SFO-tls, and SFO, as well as CRPA, are shown in Fig. 2. Averaged values of (ν, ν') and ($\bar\nu$, $\bar\nu'$) cross sections are shown for the neutral-current reaction. The elastic coherent scattering is not included. Numerical values are given in Table I. The cross sections folded over the neutrino spectra of Fermi distributions are given in Table II. The charged-current ($\bar\nu_e$, e^+) cross sections for SFO-tls are close to those of SFO, and a bit smaller than those of CRPA by 10–20% at $E_\nu = 25$–90 MeV. The neutral-current reaction cross sections for SFO-tls and CRPA are close to each other and differ only by less than 10% at $E_\nu = 30$–80 MeV.

We next investigate cross sections for separate multipolarities as a function of excitation energies E_x of the final states. Cross sections for transitions with $\lambda^\pi = 0^-$, 1^-, and 2^- as well as total ones for (ν_e, e^-), ($\bar\nu_e$, e^+), and (ν, ν') reactions obtained with SFO-tls are shown in Figs. 3–5 for $E_\nu = 30$ and 50 MeV.

We see from Figs. 3–5 that dominant contributions come from 2^- transitions at $E_x \lesssim 25$ MeV. The contributions from 0^- transitions become important around $E_x \sim 27$ MeV for $E_\nu = 30$ MeV, but the contributions from 1^- become dominant around $E_x \sim 28$ MeV for $E_\nu = 50$ MeV. These behaviors reflect the SD strengths shown in Fig. 1(a): large low-lying 2^- strength at $E_x = 0$ and 7.5 MeV, 0^- strength at $E_x \sim 13$ MeV, and 1^- strength at $E_x \sim 14.4$ MeV. Contributions from the GT (1^+) transitions are rather minor as shown in Fig. 5. They can, however, become comparable to

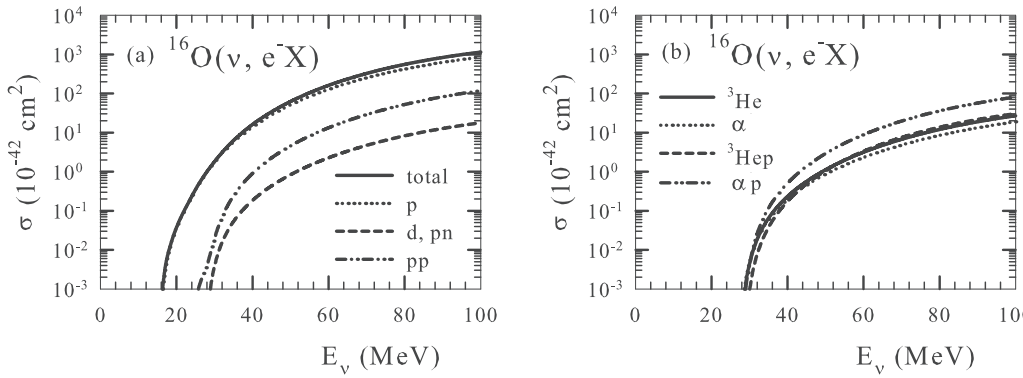

FIG. 6. Partial cross sections to various channels of ^{16}O(ν_e, e^-X) as function of neutrino energy E_ν. (a) Cases for $X = p$, d and pn, and pp as well as the total cross section are shown. (b) Cases for $X = {}^3$He (and dp, ppn), α, ^{3}Hep, and αp are shown.

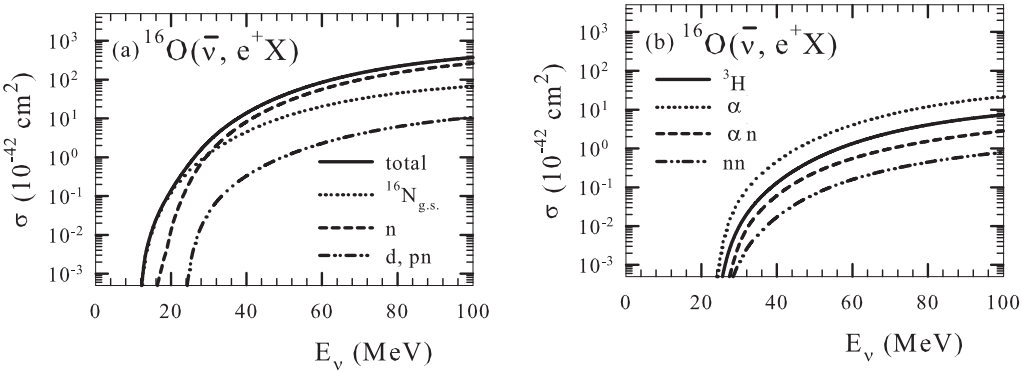

FIG. 7. The same as Fig. 6 for ^{16}O($\bar{\nu}_e$, e^+X). (a) Cases for $X = n$, d, and pn, and the transition to ^{16}N$_{g.s.}$ as well as the total cross section. (b) Cases for $X = {}^3$H (and dn, pnn), α, αn, and nn are shown.

the contributions from 0^- (and 1^-) transitions at certain E_x for $E_\nu = 30$ (50) MeV.

B. Cross sections for particle and γ emission channels

Partial cross sections for various particle and γ emission channels are evaluated by calculating the branching ratios from each excited level by the Hauser-Feshbach statistical model [29]. Single- and multiparticle decay channels involving neutron, proton, deuteron, α, ^{3}He, ^{3}H, and γ are considered. All the levels obtained in the present shell-model calculations are adopted as levels in the decaying and daughter nuclei with specific isospin assignments. The particle transmission coefficients are calculated by the optical model [30,31]. Isospin is conserved in the calculations, and possible isospin mixings are neglected. The γ-transmission coefficients are calculated with the Brink formula. The $E1$ (electric dipole) and $M1$ (magnetic dipole) parameters are taken from the RIPL-2 database [32]. The γ cascade in the initial excited nuclei and subsequent decays are fully considered.

Calculated partial cross sections for various channels obtained with the SFO-tls for ^{16}O(ν_e, e^-X), ^{16}O($\bar{\nu}_e$, e^+X), and ^{16}O(ν, $\nu'X$) reactions are shown in Figs. 6, 7, and 8, respectively. For ^{16}O(ν_e, e^-X) and ^{16}O(ν, $\nu'X$) reactions, the proton emission channel gives the dominant contribution, while for the ^{16}O($\bar{\nu}_e$, e^+X) reaction the neutron emission channel and the transition to the ground state of ^{16}N give the dominant contributions. Cross sections for various channels are given for SFO-tls in Tables III–V. Averaged cross sections folded over neutrino spectra of Fermi distributions are given in Tables VI–VIII and compared with those of CRPA. The cross sections of the single proton emission channel in the (ν_e, e^-X) reaction are enhanced by about 30–40% compared with the CRPA, while the cross sections of the single neutron emission channel in the ($\bar{\nu}_e$, e^+X) reaction are reduced by about 20% compared with the CRPA. In the case of the (ν, $\nu'X$) reaction, the cross sections for the single-proton (single-neutron) emission are enhanced (reduced) by 10% (25%) compared with the CRPA, but the sum of the cross sections of the proton and neutron emissions are close to those of the CRPA within 2%. The cross sections of the α emission channel are enhanced by about 1.7–2.2 and 2.0–2.8 times compared with the CRPA in (ν_e, e^-X) and ($\bar{\nu}_e$, e^+X) reactions, respectively. The contributions from the αp emission channel are comparable to those from pp and pn emission channels in (ν_e, e^-X) and (ν, $\nu'X$) reactions, and large compared with those of the CRPA calculation [17].

Partial cross sections for separate multipoles with 0^-, 1^-, and 2^- are also shown in Figs. 9–11 as function of excitation energy E_x for $E_\nu = 50$ MeV. Contributions other than single-proton or -neutron emissions become important at the higher excitation energy region, $E_x = 25$–30 MeV. Relatively large

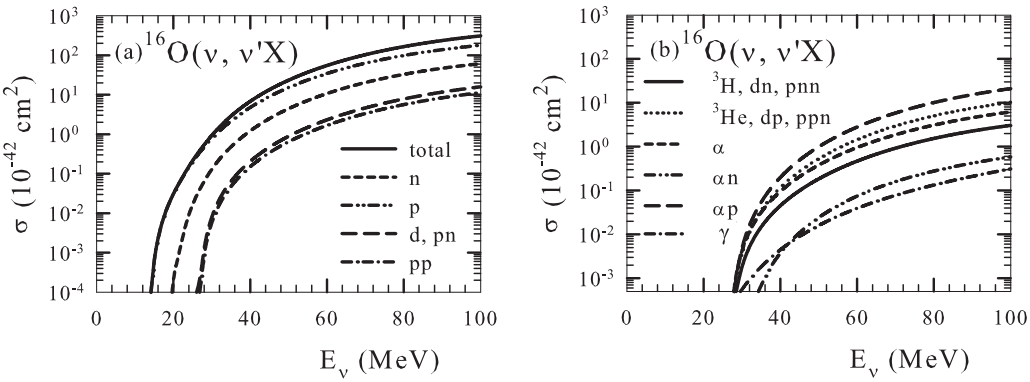

FIG. 8. The same as Fig. 6 for ^{16}O(ν, $\nu'X$). (a) Cases for $X = n$, p, d and pn, and pp as well as the total cross section. (b) Cases for $X = {}^3$H (and dn, pnn), ^{3}He (and dp, ppn), α, αn, αp, and γ are shown.

TABLE III. Partial cross sections of ^{16}O$(\nu_e, e^- X)$ for various channels obtained with the SFO-tls. The cross sections are given in units of 10^{-42} cm^2 as a function of the incoming neutrino energy E_ν. Exponents are given in parentheses.

E_ν (MeV)	p	d, pn	pp	^{3}He	α	^{3}Hep	αp
15.0	0.00	0.0	0.0	0.0	0.0	0.0	0.0
20.0	3.76(−2)	0.0	0.0	0.0	0.0	0.0	0.0
25.0	3.50(−1)	1.94(−6)	5.30(−4)	2.40(−6)	8.82(−6)	2.14(−9)	7.67(−8)
30.0	1.78(+0)	3.78(−3)	1.93(−2)	4.41(−3)	4.96(−3)	9.23(−4)	4.07(−3)
35.0	5.72(+0)	5.32(−2)	2.42(−1)	6.47(−2)	5.96(−2)	3.76(−2)	1.16(−1)
40.0	1.40(+1)	1.85(−1)	9.05(−1)	2.33(−1)	1.98(−1)	1.75(−1)	5.09(−1)
45.0	2.84(+1)	4.34(−1)	2.26(+0)	5.63(−1)	4.54(−1)	4.87(−1)	1.37(+0)
50.0	5.12(+1)	8.38(−1)	4.59(+0)	1.12(+0)	8.65(−1)	1.06(+0)	2.91(+0)
55.0	8.39(+1)	1.44(+0)	8.18(+0)	1.96(+0)	1.47(+0)	1.99(+0)	5.35(+0)
60.0	1.28(+2)	2.27(+0)	1.33(+1)	3.16(+0)	2.32(+0)	3.34(+0)	8.88(+0)
65.0	1.84(+2)	3.36(+0)	2.02(+1)	4.74(+0)	3.42(+0)	5.18(+0)	1.36(+1)
70.0	2.52(+2)	4.72(+0)	2.89(+1)	6.75(+0)	4.82(+0)	7.52(+0)	1.97(+1)
80.0	4.22(+2)	8.26(+0)	5.22(+1)	1.21(+1)	8.50(+0)	1.37(+1)	3.60(+1)
90.0	6.26(+2)	1.27(+1)	8.26(+1)	1.89(+1)	1.33(+1)	2.16(+1)	5.70(+1)
100.0	8.48(+2)	1.78(+1)	1.18(+2)	2.70(+1)	1.89(+1)	3.04(+1)	8.10(+1)

contributions from pp, αp, and α emission channels are noticed around $E_x = 30$ MeV in the $(\nu_e, e^- X)$ reaction. In the $(\bar{\nu}_e, e^+ X)$ reaction, the contributions from α and d (pn) emission channels become important around $E_x = 25$ MeV. Large contributions from the αp emission channel are also noticed at $E_x = 25$–30 MeV in the $(\nu, \nu' X)$ reaction.

IV. NUCLEOSYNTHESIS OF ^{11}B AND ^{11}C IN SN EXPLOSIONS

In Sec. III, partial cross sections in various single- and multiparticle emission channels in ν-^{16}O reactions are evaluated with the SFO-tls. Here, we study effects of the multiparticle emission channels in nucleosynthesis of light elements in core-collapse SN explosions. Comparing the cross section for ^{16}O$(\nu, \nu' \alpha p)^{11}$B with that for ^{12}C$(\nu, \nu' p)^{11}$B, which is the dominant reaction producing ^{11}B in SN explosions [4,6], its ratio becomes as large as about 10% (compare Table VIII and Fig. 2 of Ref. [6] at $T = 4$ and 8 MeV). Thus, the reaction ^{16}O$(\nu, \nu' \alpha p)^{11}$B is not negligible for nucleosynthesis of ^{11}B in SN explosions.

We calculate the nucleosynthesis of SN explosions of $M = 15 M_\odot$ and $20 M_\odot$ solar-metallicity stars. The stellar evolution of these stars is calculated in the same manner of Ref. [33]. The one-dimensional (1D) spherical SN explosions with the explosion energy of 1×10^{51} erg is calculated for 100 s using a piecewise parabolic method code as in Ref. [34]. Then, we calculate the explosive nucleosynthesis during the SN explosions by postprocessing with the neutrino process. The adopted nuclei in the nuclear reaction network are as

TABLE IV. Partial cross sections of ^{16}O$(\bar{\nu}_e, e^+ X)$ for various channels obtained with the SFO-tls. The cross sections are given in units of 10^{-42} cm^2 as a function of the incoming neutrino energy E_ν. Exponents are given in parentheses.

E_ν (MeV)	^{16}O $(\bar{\nu}_e, e^+)$ ^{16}N$_{g.s.}$	n	d, pn	^{3}H	α	αn
15.0	1.33(−2)	2.93(−5)	0.0	0.0	0.0	0.0
20.0	1.26(−1)	1.27(−2)	8.89(−7)	0.0	4.19(−7)	0.0
25.0	4.74(−1)	2.31(−1)	1.46(−3)	2.39(−4)	1.69(−3)	3.95(−5)
30.0	1.22(+0)	1.24(+0)	3.76(−2)	9.78(−3)	4.61(−2)	3.32(−3)
35.0	2.54(+0)	3.67(+0)	1.41(−1)	4.67(−2)	1.87(−1)	2.12(−2)
40.0	4.55(+0)	8.19(+0)	3.31(−1)	1.30(−1)	4.73(−1)	6.11(−2)
45.0	7.35(+0)	1.54(+1)	6.27(−1)	2.85(−1)	9.60(−1)	1.32(−1)
50.0	1.10(+1)	2.56(+1)	1.04(+0)	5.29(−1)	1.69(+0)	2.37(−1)
55.0	1.53(+1)	3.92(+1)	1.59(+0)	8.77(−1)	2.71(+0)	3.77(−1)
60.0	2.04(+1)	5.62(+1)	2.27(+0)	1.33(+0)	4.02(+0)	5.50(−1)
65.0	2.60(+1)	7.62(+1)	3.08(+0)	1.89(+0)	5.63(+0)	7.55(−1)
70.0	3.20(+1)	9.90(+1)	4.00(+0)	2.53(+0)	7.51(+0)	9.89(−1)
80.0	4.45(+1)	1.50(+2)	6.10(+0)	4.04(+0)	1.19(+1)	1.53(+0)
90.0	5.66(+1)	2.06(+2)	8.39(+0)	5.69(+0)	1.68(+1)	2.15(+0)
100.0	6.75(+1)	2.62(+2)	1.07(+1)	7.32(+0)	2.16(+1)	2.82(+0)

TABLE V. The same as in Tables III and IV for partial cross sections of ^{16}O$(\nu, \nu' X)$ for various channels obtained with the SFO-tls.

E_ν (MeV)	γ α	n αn	p αp	d, pn	pp	^{3}H	^{3}He
15.0	1.35(−7)	0.0	6.05(−4)	0.0	0.0	0.0	0.0
	1.35(−25)	0.0	0.0				
20.0	1.02(−5)	1.93(−4)	3.08(−2)	0.0	0.0	0.0	0.0
	1.47(−10)	0.0	0.0				
25.0	9.97(−5)	1.63(−2)	1.98(−1)	2.88(−5)	1.09(−5)	2.46(−9)	1.82(−5)
	1.74(−6)	0.0	4.30(−8)				
30.0	5.54(−4)	1.29(−1)	7.76(−1)	7.92(−3)	5.71(−3)	1.82(−3)	4.19(−3)
	4.14(−3)	3.76(−5)	4.83(−3)				
35.0	1.83(−3)	4.80(−1)	2.16(+0)	6.43(−2)	4.74(−2)	1.48(−2)	3.56(−2)
	3.17(−2)	6.86(−4)	5.39(−2)				
40.0	4.46(−3)	1.22(+0)	4.76(+0)	2.06(−1)	1.51(−1)	4.52(−2)	1.18(−1)
	9.55(−2)	3.74(−3)	1.99(−1)				
45.0	9.00(−3)	2.49(+0)	9.01(+0)	4.68(−1)	3.41(−1)	9.96(−2)	2.75(−1)
	2.07(−1)	1.09(−2)	4.96(−1)				
50.0	1.60(−2)	4.44(+0)	1.52(+1)	8.87(−1)	6.44(−1)	1.85(−1)	5.36(−1)
	3.81(−1)	2.43(−2)	9.97(−1)				
55.0	2.60(−2)	7.17(+0)	2.37(+1)	1.49(+0)	1.08(+0)	3.06(−1)	9.23(−1)
	6.27(−1)	4.53(−2)	1.75(+0)				
60.0	3.94(−2)	1.07(+1)	3.45(+1)	2.31(+0)	1.68(+0)	4.69(−1)	1.45(+0)
	9.57(−1)	7.48(−2)	2.80(+0)				
65.0	5.66(−2)	1.52(+1)	4.77(+1)	3.36(+0)	2.43(+0)	6.75(−1)	2.14(+0)
	1.37(+0)	1.13(−1)	4.17(+0)				
70.0	7.78(−2)	2.04(+1)	6.29(+1)	6.64(+0)	3.35(+0)	9.24(−1)	2.97(+0)
	1.87(+0)	1.60(−1)	5.85(+0)				
80.0	1.34(−1)	3.28(+1)	9.86(+1)	7.82(+0)	5.63(+0)	1.54(+0)	5.06(+0)
	3.11(+0)	2.78(−1)	1.01(+1)				
90.0	2.10(−1)	4.68(+1)	1.38(+2)	1.17(+1)	8.36(+0)	2.27(+0)	7.57(+0)
	4.58(+0)	4.23(−1)	1.53(+1)				
100.0	3.12(−1)	6.11(+1)	1.79(+2)	1.59(+1)	1.13(+1)	3.06(+0)	1.03(+1)
	6.20(+0)	5.85(−1)	2.11(+1)				

follows: $^{1-3}$H, ^{3,4}He, ^{6,7}Li, ^{7,9}Be, ^{8,10,11}B, $^{11-16}$C, $^{13-18}$N, $^{14-20}$O, $^{17-22}$F, $^{18-24}$Ne, $^{21-26}$Na, $^{22-28}$Mg, $^{27-32}$Si, $^{27-34}$P, $^{30-37}$S, $^{32-38}$Cl, $^{34-43}$Ar, $^{36-45}$K, $^{38-48}$Ca, $^{40-49}$Sc, $^{42-51}$Ti, $^{44-53}$V, $^{46-55}$Cr, $^{48-57}$Mn, $^{50-61}$Fe, $^{51-62}$Co, $^{54-66}$Ni, $^{56-68}$Cu, $^{59-71}$Zn, $^{61-71}$Ga, $^{63-75}$Ge, $^{65-76}$As, $^{67-77}$Se, and $^{70-79}$Br. The total neutrino energy is set to be 3×10^{53} erg. The neutrino luminosity is assumed to decay exponentially in time with a time scale of 3 s and is equally partitioned among three flavors of neutrinos and antineutrinos. The neutrino energy spectra are assumed to obey Fermi distributions with zero chemical

TABLE VI. Averaged cross sections of ^{16}O$(\nu_e, e^- X)$ folded over Fermi distributions of neutrino spectra with temperatures $T = 4$ and 8 MeV obtained with the SFO-tls and CRPA. The cross sections are given in units of 10^{-42} cm^2 as a function of the temperature. Exponents are given in parentheses. In the case of $X = p$, values in the parentheses are those for the transitions to ^{15}O$_{g.s.}$.

Neutrino reactions	$T = 4$ MeV		$T = 8$ MeV	
	SFO-tls	CRPA	SFO-tls	CRPA
Total	2.59(−1)	1.91(−1)	1.53(+1)	1.37(+1)
^{16}O$(\nu, e^- p)^{15}$O	2.29(−1)	1.62(−1) (1.21(−1))	1.22(+1)	9.56(+0) (6.37(+0))
^{16}O$(\nu, e^- np)^{14}$O	2.36(−3)	3.92(−4)	2.08(−1)	1.76(−1)
^{16}O$(\nu, e^- pp)^{14}$N	1.21(−2)	2.61(−2)	1.22(+0)	3.26(+0)
^{16}O$(\nu, e^- {}^3$He$)^{13}$N	3.04(−3)		2.90(−1)	
^{16}O$(\nu, e^- \alpha)^{12}$N	2.52(−3)	1.16(−3)	2.16(−1)	1.31(−1)
^{16}O$(\nu, e^- {}^3$He$p)^{12}$C	2.47(−3)		3.00(−1)	
^{16}O$(\nu, e^- \alpha p)^{11}$C	7.00(−3)	2.17(−3)	8.06(−1)	5.66(−1)

TABLE VII. Averaged cross sections of ^{16}O($\bar{\nu}_e$, e^+X) folded over Fermi distributions of neutrino spectra with temperatures $T = 5$ and 8 MeV obtained with the SFO-tls and CRPA. The cross sections are given in units of 10^{-42} cm^2 as a function of the temperature. Exponents are given in parentheses. In the case of $X = n$, values in the parentheses are those for the transitions to ^{15}N$_{g.s.}$.

Neutrino reactions	$T = 5$ MeV		$T = 8$ MeV	
	SFO-tls	CRPA	SFO-tls	CRPA
Total	9.44(−1)	1.05(+0)	8.66(+0)	9.63(+0)
^{16}O($\bar{\nu}$, e^+)^{16}N	3.51(−1)	4.94(−1) (3.47(−1))	2.37(+0)	4.05(+0) (2.15(+0))
^{16}O($\bar{\nu}$, e^+n)^{15}N	5.29(−1)	6.71(−1) (5.24(−1))	5.49(+0)	6.71(+0) (4.81(+0))
^{16}O($\bar{\nu}$, e^+np)^{14}C	1.99(−2)	4.56(−3)	2.20(−1)	1.38(−1)
^{16}O($\bar{\nu}$, e^+nn)^{14}N	1.09(−3)	5.50(−3)	1.42(−2)	1.81(−1)
^{16}O($\bar{\nu}$, $e^+{}^3$H)^{13}C	8.64(−3)		1.19(−1)	
^{16}O($\bar{\nu}$, e^+ α)^{12}B	2.99(−2)	1.07(−2)	3.75(−1)	1.91(−1)
^{16}O($\bar{\nu}$, e^+ αn)^{11}B	3.78(−3)	6.20(−3)	4.97(−2)	2.16(−1)

potentials. The temperatures of ν_e, $\bar{\nu}_e$, and $\nu_x = \nu_{\mu,\tau}$ and $\bar{\nu}_{\mu,\tau}$ are set to be $(T_{\nu_e}, T_{\bar{\nu}_e}, T_{\nu_x}) = (4, 4, 6)$ MeV.

To clarify the effect of the new cross section and branches of the ν-^{16}O reactions, we consider three cases of the nucleosynthesis calculations. In case 1, only single n, p, α, and γ emission channels are considered with previous HW92 cross sections [7]. New cross sections for ^{4}He and ^{12}C in Ref. [6] are also used. In case 2, the present new cross sections obtained with the SFO-tls are used, but with only single-particle and γ emission channels. In case 3, the multiparticle branches are included with the present new cross sections for ^{16}O.

The production yields of ^{11}B as well as ^{11}C are estimated with the inclusion of the ^{16}O(ν, $\nu'\alpha p$)^{11}B and ^{16}O(ν_e, $e^-\alpha p$)^{11}C reactions for the SN explosion models. Calculated production yields are given in Table IX. We see from Table IX that the production yields of the sum of ^{11}B and ^{11}C are enhanced by about 10% when the multiparticle channels are included.

Mass fraction distributions of ^{11}B and ^{11}C for the three cases as well as main elements are shown in Figs. 12 and 13 for the SN explosions of $M = 15M_\odot$ and $M = 20M_\odot$ stars, respectively. ^{11}B is produced mainly through the ^{12}C(ν, $\nu' p$)^{11}B reaction in the O/Ne layer and ^{4}He(ν, $\nu' p$)^{3}H(α, γ)^{7}Li(α, γ)^{11}B in the He/C layers as we see from Figs. 12(a) and 12(b) and Figs. 13(a) and 13(b). ^{11}B is also produced in the O/Ne layer through the ^{16}O(ν, $\nu'\alpha p$)^{11}B reaction, which enhances the mass fraction of ^{11}B in the O/Ne layer as seen in Figs. 12(b) and 13(b). ^{11}C is produced mainly through the ^{12}C(ν, $\nu' n$)^{11}C reaction in the He/C and the O/Ne layers. It is produced also through the ^{12}C(ν_e, $e^- p$)^{11}C reaction, and the ^{16}O(ν_e, e^- αp)^{11}C reaction in the O/Ne layer. The cross section for the latter charged-current reaction on ^{16}O is about 4% of that of the former one on ^{12}C at $T = 4$ MeV, while the mass fraction of ^{16}O is larger than that of ^{12}C by about 20 (8) times in the O/Ne layer for $M = 15M_\odot$ ($20M_\odot$). This leads to similar production rates for the two charged-current reactions in the O/Ne layer in the case of $M = 15M_\odot$, but less production rate for the charged-current reaction on ^{16}O compared with that on ^{12}C in the case of $M = 20M_\odot$. Additional contributions come from a neutral current reaction ^{16}O(ν, $\nu'\alpha n$)^{11}C induced by ν_x's with higher temperature $T = 6$ MeV. These multiparticle emission

TABLE VIII. Averaged cross sections of ^{16}O(ν, $\nu' X$) folded over Fermi distributions of neutrino spectra with temperatures $T = 4$, 6, and 8 MeV obtained with the SFO-tls and CRPA. The cross sections are given in units of 10^{-42} cm^2 as a function of the temperature. Exponents are given in parentheses. In the case of $X = n$ ($X = p$), values in the parentheses are those for the transitions to ^{15}O$_{g.s.}$ (^{15}N$_{g.s.}$).

Neutrino reactions	$T = 4$ MeV	$T = 6$ MeV	$T = 8$ MeV	
	SFO-tls	SFO-tls	SFO-tls	CRPA
Total	1.15(−1)	1.28(+0)	5.29(+0)	5.19(+1)
^{16}O(ν, $\nu'\gamma$)^{16}O	7.16(−5)	8.73(−4)	3.88(−3)	3.19(−3)
^{16}O(ν, $\nu' n$)^{15}O	1.81(−2)	2.31(−1)	1.00(+0)	1.32(+0) (9.73(−1))
^{16}O(ν, $\nu' p$)^{15}N	8.66(−2)	8.66(−1)	3.40(+0)	3.14(+0) (1.85(+0))
^{16}O(ν, $\nu' np$)^{14}N	2.66(−3)	4.37(−2)	2.10(−1)	4.40(−1)
^{16}O(ν, $\nu' pp$)^{14}C	1.94(−3)	3.17(−2)	1.52(−1)	8.35(−2)
^{16}O(ν, $\nu'{}^3$H)^{13}N	5.77(−4)	9.12(−3)	7.45(−2)	
^{16}O(ν, $\nu'{}^3$He)^{13}C	1.55(−3)	2.65(−2)	1.31(−1)	
^{16}O(ν, $\nu'\alpha$)^{12}C	1.22(−3)	1.89(−2)	8.77(−2)	
^{16}O(ν, $\nu'\alpha n$)^{11}C	5.38(−5)	1.17(−3)	6.43(−3)	3.88(−2)
^{16}O(ν, $\nu'\alpha p$)^{11}B	2.65(−3)	4.89(−2)	2.50(−1)	9.15(−2)

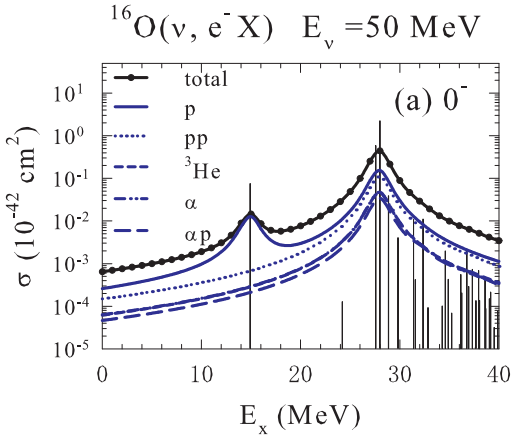

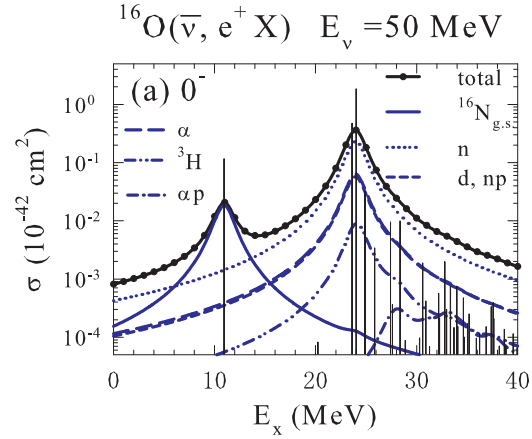

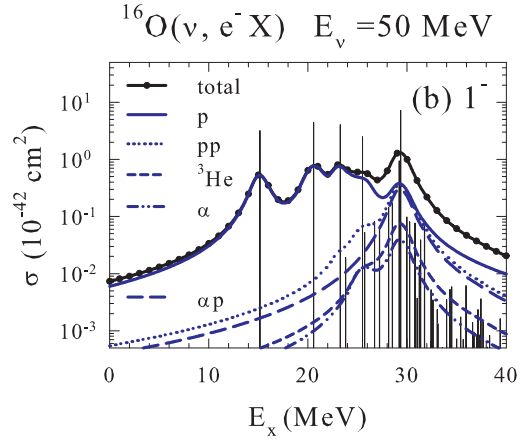

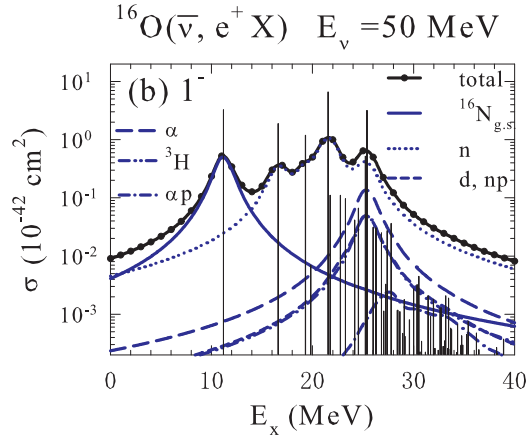

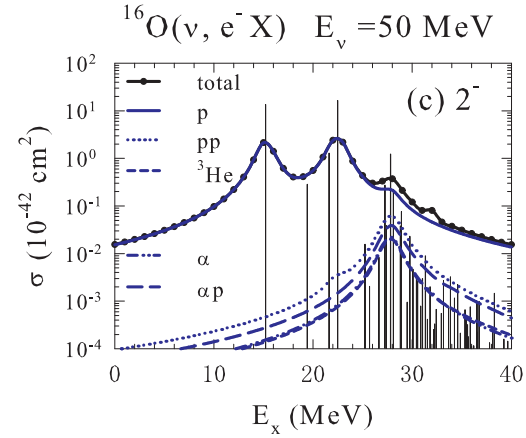

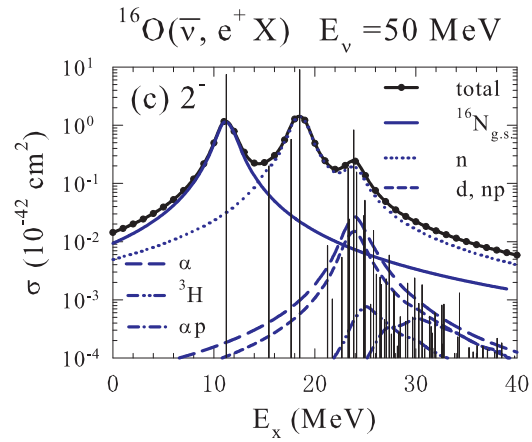

FIG. 9. Partial cross sections for ^{16}O(ν_e, e^-X) for each multipole (a) 0^-, (b) 1^-, and 2^- as function of E_x for $E_\nu = 50$ MeV. Cases for $X = p$, pp, ^{3}He, α, and αp as well as the total cross section are shown.

FIG. 10. The same as Fig. 9 for ^{16}O ($\bar{\nu}_e$, e^+X). Cases for $X = n$, d or pn, α, ^{3}H, αp, and the transition to ^{16}O$_{g.s.}$ are shown.

TABLE IX. Production yields of ^{11}B and ^{11}C in SN explosions for progenitor mass of $M = 15M_\odot$ and $20M_\odot$.

Production yield ($10^{-7}M_\odot$)	M=15$M_\odot$			M=20$M_\odot$		
	Case 1	Case 2	Case 3	Case 1	Case 2	Case 3
M(^{11}B)	2.94	2.92	3.13	6.77	6.58	7.66
M(^{11}C)	2.80	2.71	3.20	9.33	8.91	9.64
M(^{11}B +^{11}C)	5.74	5.62	6.33	16.10	15.49	17.29

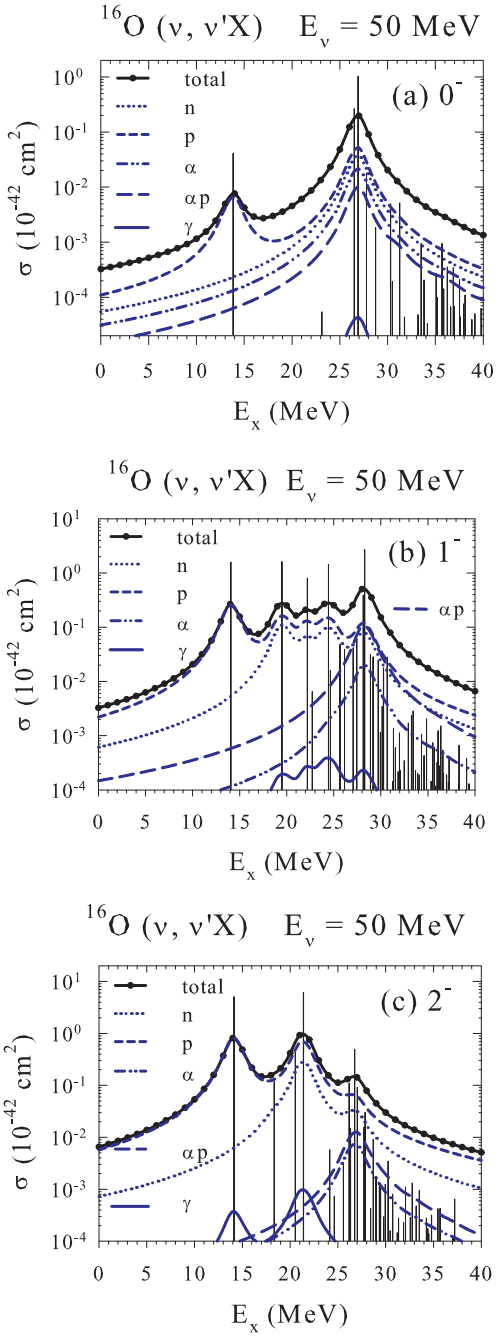

FIG. 11. The same as Fig. 10 for ^{16}O(ν, $\nu' X$). Cases for $X = n$, p, α, αp, and γ are shown.

channels lead to an enhancement of ^{11}C in the O/Ne layer. As ^{11}B is destroyed by the ^{11}B$(p, \alpha\alpha)^4$He reaction in the O/Ne layer, ^{11}C is more produced than ^{11}B in the O/Ne layer. Production yields of light elements, ^{6}Li, ^{7}Li, ^{7}Be, ^{9}Be, and ^{10}B, in the core-collapse SN explosions are also given in Table X, which shows effects of the new cross sections and the multiparticle channels, and their mass fraction distributions in case 3 are shown in Figs. 12(d) and 13(d).

V. SUMMARY

We have studied ν-induced reactions on ^{16}O by shell-model calculations with the new Hamiltonian, SFO-tls [20]. Spin-dipole transitions are investigated as dominant contributions to the ν-^{16}O reaction cross sections coming from these transition strengths with the multipolarities, 0^-, 1^-, and 2^-. The spin-dipole strengths obtained with the SFO-tls are shifted toward the lower-energy region compared with the SFO [3]. The quenching of g_A in the spin-dipole transitions is studied by the muon-capture reaction on ^{16}O. Total muon-capture rates obtained for the SFO and SFO-tls are found to agree with the experimental value within 10% with the use of the quenching factor $f = 0.95$, which is used in the present calculations.

Total as well as partial cross sections to various single- and multiparticle emission channels are evaluated by using the branching ratios obtained by the Hauser-Feshbach statistical model. In the present calculation, the isospin conservation is fully taken into account.

The total (ν_e, e^-) cross section, partial cross sections for α emission channels, especially the αp emission channel, in (ν_e, e^-) and (ν, ν') reactions are found to be enhanced compared with the standard CRPA calculations. Effects of the inclusion of various multiparticle emission channels on nucleosynthesis of light elements in core-collapse SN explosions are investigated. The αp emission channels such as ^{16}O$(\nu, \nu'\alpha p)^{11}$B and ^{16}O$(\nu_e, e^- \alpha p)^{11}$C reactions are found to lead to an enhancement of the production yields of ^{11}B and ^{11}C by about 10% compared to the case with only single-nucleon emissions from ^{12}C.

In Ref. [35], based on the present work, event spectra of the charged-current reactions as a function of recoil energy of e^-/e^+ are discussed for future SN neutrino detection at the Super-Kamiokande. The dependence on various SN neutrino spectra in addition to the Fermi distribution as well as on neutrino mass hierarchies are also discussed. Future

TABLE X. Production yields of ^{6}Li, ^{7}Li, ^{7}Be, ^{9}Be, and ^{10}B in SN explosions for progenitor mass of $M = 15M_\odot$ and $20M_\odot$. They are given in units of $M_\odot$. Exponents are given in parentheses.

Production yield ($M_\odot$)	M=15$M_\odot$			$M = 20M_\odot$		
	Case 1	Case 2	Case 3	Case 1	Case 2	Case 3
M(^{6}Li)	4.29(−11)	4.16(−11)	4.39(−11)	2.33(−10)	2.19(−10)	2.90(−10)
M(^{7}Li)	7.23(−8)	7.23(−8)	7.09(−8)	1.11(−7)	1.10(−7)	1.02(−7)
M(^{7}Be)	2.33(−7)	2.33(−7)	2.33(−7)	2.57(−7)	2.57(−7)	2.61(−7)
M(^{9}Be)	9.62(−11)	9.50(−11)	1.01(−10)	4.12(−10)	3.81(−10)	6.93(−10)
M(^{10}B)	2.18(−9)	2.12(−9)	2.42(−9)	6.71(−9)	6.15 (−9)	6.47(−9)

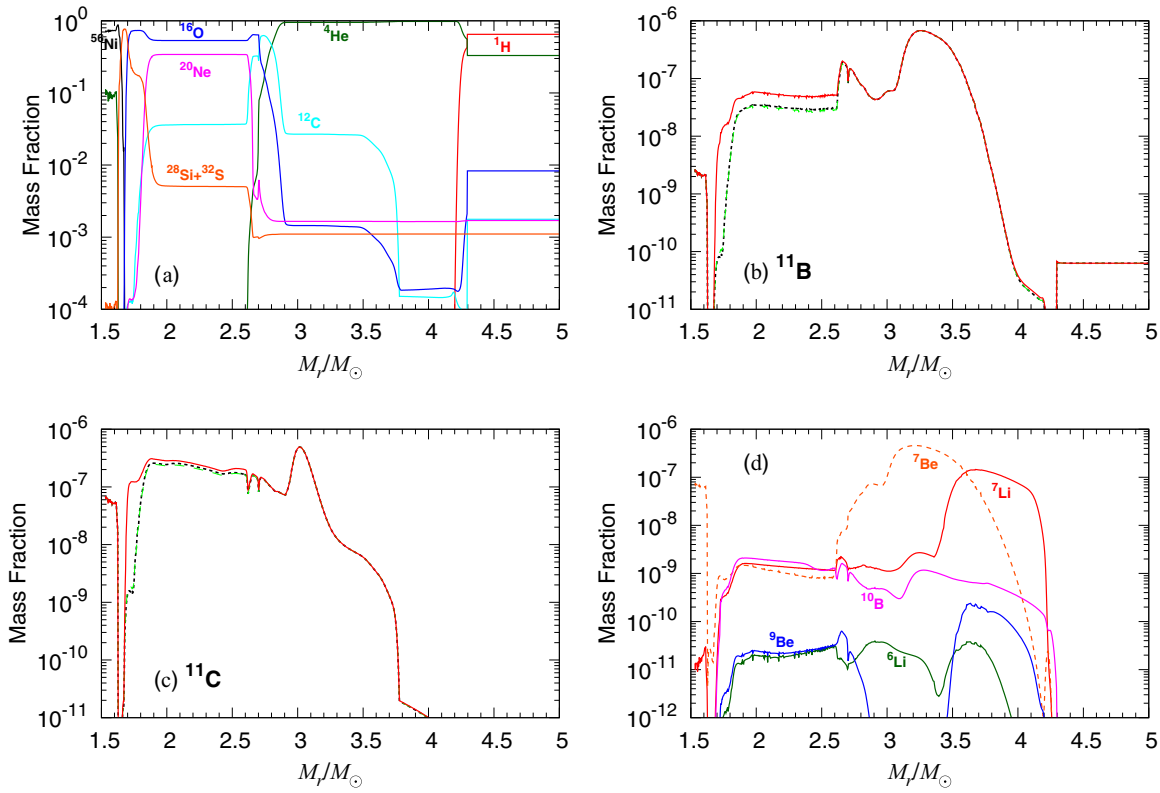

FIG. 12. Mass fraction distributions of (a) main elements, (b) ^{11}B, (c) ^{11}C, and (d) ^{6}Li, ^{7}Li, ^{7}Be, ^{9}Be, and ^{10}B for a model with $M = 15M_\odot$. The horizontal axis denotes the cumulative mass of the star from the center in the solar mass unit $M_\odot$. Short-dashed, long-dashed, and solid curves in (b) and (c) are for cases 1, 2, and 3, respectively (see text). Curves in (d) are for case 3.

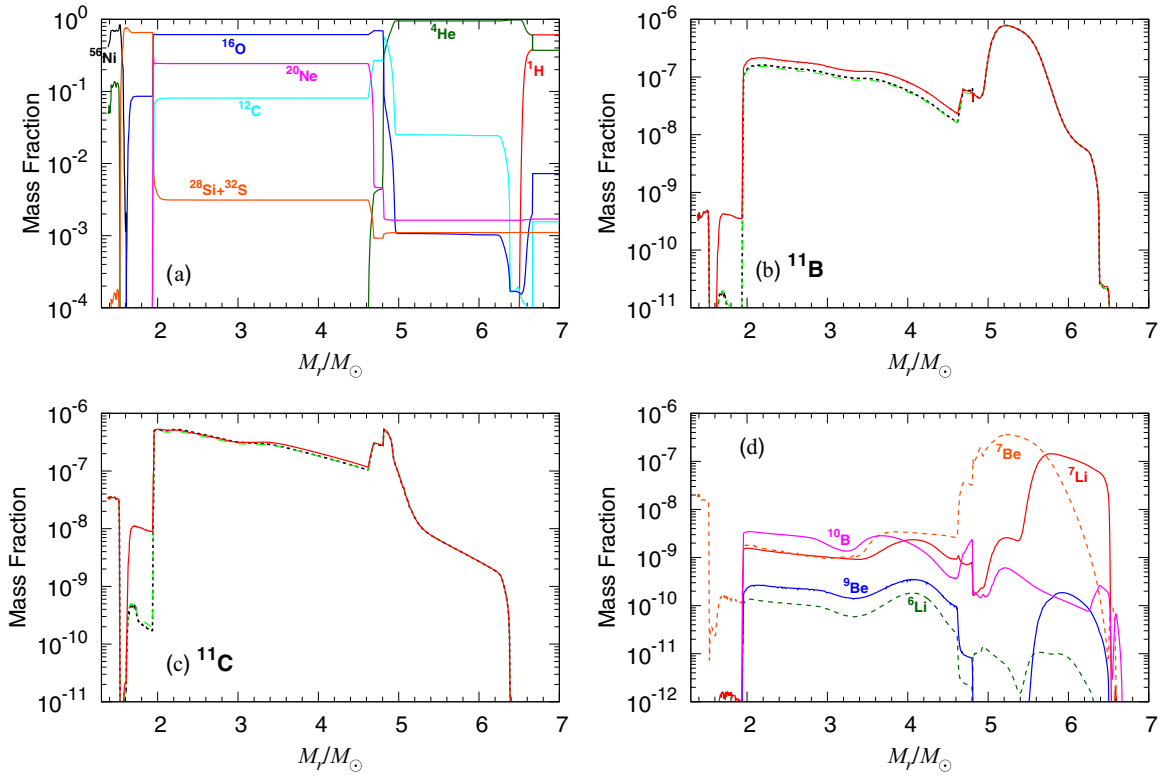

FIG. 13. The same as Fig. 12 for $M = 20M_\odot$.

SN neutrino detection at Hyper-Kamiokande is discussed in Ref. [36].

There are also recent works concerning SN neutrino detection as well as ν process nucleosynthesis in SN explosions. In Ref. [37], the reduction of the high-energy tail of the spectrum of core-collapse SN ν_e produced by neutronization burst is discussed, and important effects in ν-^{16}O reactions are pointed out. Roles of the ν process in explosive SN nucleosynthesis are investigated including neutrino-nucleus reactions for all nuclei with $Z < 76$ and using neutrino spectra in agreement with modern SN simulations, which give significantly reduced neutrino energies compared with the previous ones [38]. Experimental techniques for the detection of SN neutrinos and the sensitivities of the detectors are reviewed in Ref. [39]. Various possible signatures of neutrino mass hierarchies by observed SN neutrino events at earth as well as their robustness are surveyed in Ref. [40]. Thus, various applications to low-energy neutrino detection and nucleosynthesis in stars can be carried out based on the present new reaction cross sections.

ACKNOWLEDGMENTS

The authors would like to thank M. Sakuda and K. Nakazato for useful discussion on experiments and experimental plans at Super- and Hyper-Kamiokande and RCNP. This work has been supported in part by JSPS KAKENHI Grant No. JP15K05090. K.T. was supported by the JSPS Overseas Research Fellowships.

[1] T. Otsuka, T. Suzuki, R. Fujimoto, H. Grawe, and Y. Akaishi, Phys. Rev. Lett. **95**, 232502 (2005).
[2] T. Otsuka, T. Suzuki, M. Honma, Y. Utsuno, N. Tsunoda, K. Tsukiyama, and M. Hjorth-Jensen, Phys. Rev. Lett. **104**, 012501 (2010).
[3] T. Suzuki, R. Fujimoto, and T. Otsuka, Phys. Rev. C **67**, 044302 (2003).
[4] T. Suzuki, S. Chiba, T. Yoshida, T. Kajino, and T. Otsuka, Phys. Rev. C **74**, 034307 (2006).
[5] T. Suzuki and T. Kajino, J. Phys. G **40**, 083101 (2013).
[6] T. Yoshida, T. Kajino, T. Suzuki, S. Chiba, T. Otsuka, A. Takamura, K. Kimura, H. Yokomakura, and D. H. Hartmann, Astrophys. J. **686**, 448 (2008).
[7] S. E. Woosley, D. H. Hartmann, R. D. Hoffman, and W. C. Haxton, Astrophys. J. **356**, 272 (1990).
[8] T. Yoshida, T. Kajino, and D. H. Hartmann, Phys. Rev. Lett. **94**, 231101 (2005).
[9] T. Suzuki, A. B. Balantekin, and T. Kajino, Phys. Rev. C **86**, 015502 (2012).
[10] J. Arafune, M. Fukugita, Y. Kohyama, and K. Kubodera, Phys. Lett. B **217**, 186 (1989).
[11] Y. Utsuno, T. Otsuka, T. Mizusaki, and M. Honma, Phys. Rev. C **60**, 054315 (1999).
[12] M. Honma, T. Otsuka, T. Mizusaki, M. Hjorth-Jensen, and B. A. Brown, J. Phys.: Conf. Ser. **20**, 7 (2005).
[13] M. Bhattacharya, C. D. Goodman, and A. Garcia, Phys. Rev. C **80**, 055501 (2009).
[14] T. Suzuki and M. Honma, Phys. Rev. C **87**, 014607 (2013).
[15] W. E. Ormand, P. M. Pizzochero, P. F. Bortignon, and R. A. Broglia, Phys. Lett. B **345**, 343 (1995).
[16] E. Kolbe, K. Langanke, G. Martínez-Pinedo, and P. Vogel, J. Phys. G **29**, 2569 (2003); I. Gil-Botella and A. Rubbia, J. Cosmol. Astropart. Phys. **10**, 9 (2003).
[17] K. Langanke, P. Vogel, and E. Kolbe, Phys. Rev. Lett. **76**, 2629 (1996); E. Kolbe, K. Langanke, and P. Vogel, Phys. Rev. D **66**, 013007 (2002).
[18] D. J. Millener and D. Kurath, Nucl. Phys. A **255**, 315 (1975).
[19] G. Bertsch, J. Borysowicz, H. McManus, and W. G. Love, Nucl. Phys. A **284**, 399 (1977).
[20] T. Suzuki and T. Otsuka, Phys. Rev. C **78**, 061302 (2008).
[21] T. Otsuka, A. Gade, O. Sorlin, T. Suzuki, and Y. Utsuno, arXiv:1805.06501.
[22] National Nuclear Data Center, http://www.nndc.bnl.gov/.
[23] T. Suzuki and H. Sagawa, Nucl. Phys. A **637**, 547 (1998).
[24] T. Suzuki, Nucl. Phys. A **687**, 119c (2001).
[25] A. Bohr and B. R. Mottelson, *Nuclear Structure* (Benjamin, New York, 1969), Vol. I.
[26] J. D. Walecka, in *Muon Physics*, edited by V. H. Hughes and C. S. Wu (Academic, New York, 1975), Vol. II; J. S. O'Connell, T. W. Donnelly, and J. D. Walecka, Phys. Rev. C **6**, 719 (1972); T. W. Donnelly and J. D. Walecka, Nucl. Phys. A **274**, 368 (1976).
[27] T. Suzuki, D. F. Measday, and J. P. Roalsvig, Phys. Rev. C **35**, 2212 (1987).
[28] E. Kolbe, K. Langanke, and P. Vogel, Phys. Rev. C **50**, 2576 (1994).
[29] W. Hauser and H. Feshbach, Phys. Rev. **87**, 366 (1952).
[30] R. L. Walter and P. P. Guss, in *Proceedings of the International Conference on Nuclear Data for Basic and Applied Science*, edited by P. G. Young, Vol. 2 (Gordon and Breach, New York, 1986), p. 1079.
[31] V. Avrigeanu, P. E. Hodgson, and M. Avrigeanu, Phys. Rev. C **49**, 2136 (1994).
[32] T. Belgya, O. Bersillon, R. Capote, T. Fukahori, G. Zhigang, S. Goriely, M. Herman, A. V. Ignatyuk, S. Kailas, A. Koning, P. Oblozhinsky, V. Plujko, and P. Young, *Handbook for Calculations of Nuclear Reaction Data: Reference Input Parameter Library* (IAEA, Vienna, 2006), http://wwwnds.iaea.org/RIPL-2/.
[33] T. Yoshida, S. Okita, and H. Umeda, Mon. Not. R. Astron. Soc. **438**, 3119 (2014).
[34] H. Umeda and K. Nomoto, Astrophys. J. **619**, 427 (2005).
[35] K. Nakazato, T. Suzuki, and M. Sakuda, arXiv:1809.08398.
[36] K. Abe *et al.* (Hyper-Kamiokande proto collaboration), arXiv:1805.04163.
[37] K. Langanke and G. Martínez-Pinedo, J. Phys.: Conf. Ser. **940**, 012002 (2018).
[38] A. Sieverding, G. Martínez-Pinedo, L. Huther, K. Langanke, and A. Heger, arXiv:1805.10231.
[39] K. Scholberg, Annu. Rev. Nucl. Part. Sci. **62**, 81 (2012).
[40] K. Scholberg, J. Phys. G **45**, 014002 (2018).